LBL-18745
Preprint

Lawrence Berkeley Laboratory
UNIVERSITY OF CALIFORNIA

Physics Division

Submitted to Nuovo Cimento

NEW MEASUREMENTS OF THE COSMIC BACKGROUND RADIATION SPECTRUM

G.F. Smoot, G. De Amici,
S. Levin, and C. Witebsky

December 1984

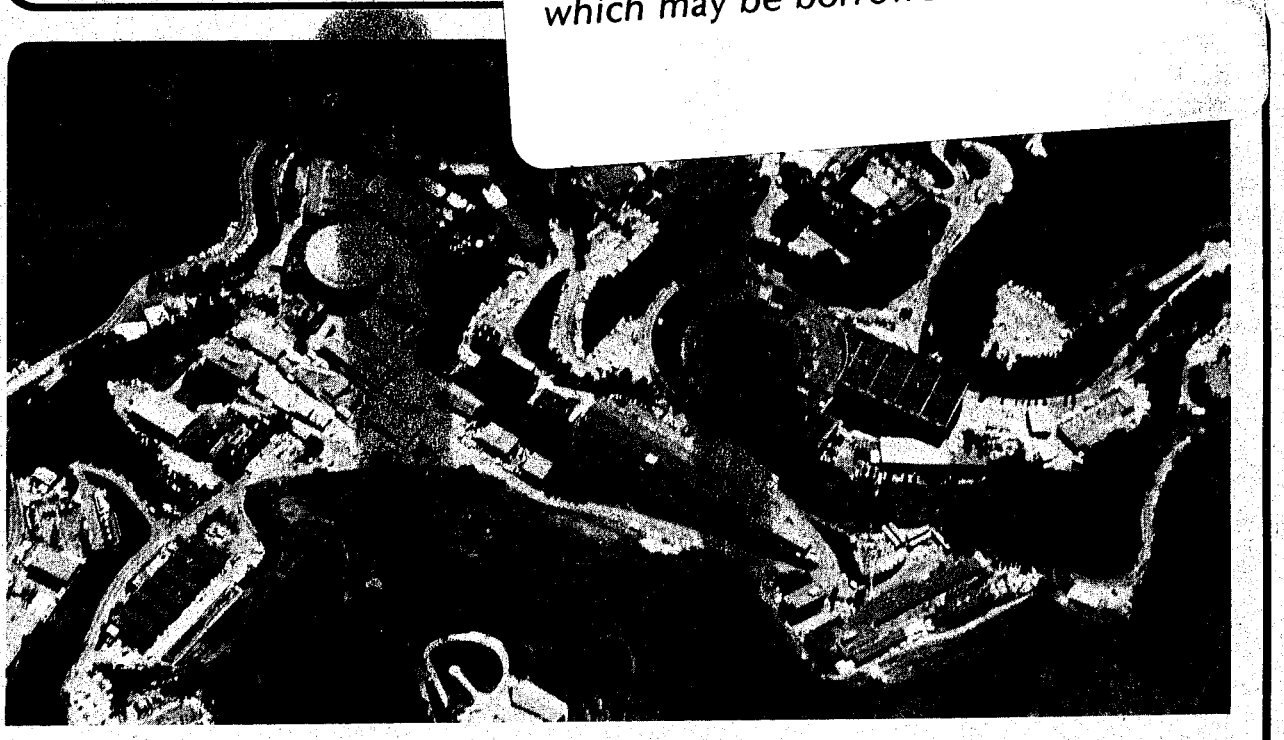

Prepared for the U.S. Department of Energy under Contract DE-AC03-76SF00098

NEW MEASUREMENTS OF THE COSMIC BACKGROUND RADIATION SPECTRUM

GEORGE F. SMOOT, GIOVANNI DE AMICI, STEVE LEVIN, AND CHRIS WITEBSKY
Spaces Sciences Laboratory and Lawrence Berkeley Laboratory
University of California, Berkeley, CA 94720

(ricevuto il 11 Dec 1984)

Summary. – We have continued our program to measure the long-wavelength spectrum of the cosmic background radiation. Our previous observations were at five wavelengths – 0.33, 0.9, 3.0, 6.3, and 12.0 cm – and had a weighted average value of 2.73 ± 0.05 K and deviated from a Planckian spectrum by less than 6%. In August 1984, we repeated our observations at 3.0, 0.9, and 0.33 cm and made new observations with a radiometer tunable from 1.7 to 15 cm. Preliminary analysis indicate that the new data are consistent with our previous results.

PACS. 98.70.Vc, 98.80.Bp – Cosmic Background Radiation Spectrum

1. – INTRODUCTION

The Cosmic Background Radiation (CBR) is one of the few observables that retains information about the early universe, but there are limits to its memory. In the standard Big Bang model the universe is opaque at redshifts z greater than about 1000. For times after $z \approx 1000$ the matter in the universe is mostly in neutral atoms and the optical depth (due primarily to Rayleigh scattering) is much longer than the present Hubble radius (10^{10} light years). Before a redshift of 1000 the matter is in the form of primordial plasma, because the temperature is greater than 3000 K so that the hydrogen and helium are ionized. Just before this boundary the primary interaction between the CBR and matter is through Compton (Thomson) scattering of the photons by free electrons. The angular distribution for low-energy Compton scattering is nearly isotropic so that directional information is practically erased by a single scattering. Polarization information is lost nearly as quickly. Before recombination ($1000 < z < 1500$) the universe and its contents are obscured by a cosmic fog bank. Objects in the foreground, such as stars, galaxies, and quasars, can be imaged conventionally and clearly. Objects in the boundary are hazy and ill-defined. Objects in the background before the boundary are obscured and hidden from view. The angular distribution of the CBR thus carries information on the large-scale structure of the universe and the inhomogeneities in the matter distribution at the surface of last scattering. Earlier information is lost.

Compton scattering does not alter the CBR's spectrum as effectively as it mixes the radiation direction. This is because Compton scattering preserves the number of photons and because on the average it changes the energy of the photon by a fractional amount comparable to the ratio of the electron's kinetic energy to its rest mass, kT_e/m_ec^2. At the boundary ($z \approx 1000$) this factor is about 10^{-6}. Thus just before decoupling one scattering can change a photon's direction by a large angle; in contrast it would take about a million scatterings to change its energy by a large fraction. Compton scattering can effectively alter the CBR spectrum only at much higher temperatures and densities. The temperature and thus the electron kinetic energy scale as $(1 + z)$ and the number density of electrons scales as $(1 + z)^3$. At redshifts greater than a few times 10^4 there are sufficient scatterings and kinetic energy to thermalize the spectrum. However, since Compton scattering preserves the number of photons, the thermalized spectrum would be a Bose-Einstein distribution. One must go to even higher temperatures and densities to find processes that can effectively change the photon number. Radiative Compton scattering and bremsstrahlung (free-free emission) become important at redshifts greater than about 10^6. Both processes produce low-energy photons which must be Compton

scattered to much higher frequencies. At redshifts greater than 10^8 the temperature is sufficiently high that electron-positron pair production and annihilation take place readily. In this regime a Planckian spectrum can be established on a time scale short compared to the expansion and cooling of the universe. We therefore can conclude that the CBR spectrum does not retain any information about the universe for times before a redshift of 10^7 to 10^8, except that it was hot (Illarionov and Sunyaev 1975, Danese and De Zotti 1977, 1978, and 1982).

The spectrum of the CBR contains information about the energy-releasing processes in the universe for the time period beginning about a year after the start of the Big Bang. A number of processes may have released energy into the universe during this period. These include large scale motions of the matter such as turbulence, shock waves, and fragmentation of protogalaxies or protoclusters, irregularities and inhomogeneities in the matter distribution, the annihilation of matter and antimatter, or the decay of long-lived particles. Accurate measurements of the CBR spectrum restrict any theory involving injection of energy into the radiation field, since energy release would have distorted the CBR spectrum from its initial blackbody distribution. These distortions are expected to have their maximum deviation from a blackbody spectrum in the wavelength range of a few centimeters.

Realizing that a significant ($\approx$15%) distortion could have gone undetected, we have undertaken a program to measure the low-frequency spectrum of the CBR. Previous results have been reported by Smoot *et al.* (1983, 1984). This paper presents the results of a new set of observations made with fixed-frequency radiometers at wavelengths of 0.33, 0.9, and 3.0 cm and with a new broadband radiometer which is tunable from 1.7 to 15 cm.

2. – CONCEPTS AND REQUIREMENTS OF THE MEASUREMENT

The intensity of the CBR is measured at each frequency by a radiometer, a device whose output voltage is proportional to the power intercepted by its antenna. The radiometer is calibrated in units of antenna temperature (a measure of intercepted power) per voltage output by measuring the change in output voltage for a known change in input antenna temperature. The calibration targets are microwave absorbers at ambient temperature and in baths of liquid nitrogen or liquid helium.

The antenna temperature T_A is proportional to the input power P according to the relation

$$P = kT_A B \tag{1}$$

and is related to the thermodynamic temperature T of a blackbody source covering the antenna aperture by

$$T_A = \frac{T_\nu}{(e^{T_\nu/T} - 1)}, \tag{2}$$

where $T_\nu = h\nu/k = 0.048\nu$ (K/GHz), h is Planck's constant, ν is frequency, k is Boltzmann's constant, and B is the radiometer bandwidth. At low frequencies ($T_\nu << T$) the antenna temperature is nearly equal to the thermodynamic temperature.

Each CBR measurement compares the antenna temperature of the zenith with that of an absolute-reference blackbody load of known temperature. The zenith antenna temperature can be expressed as

$$T_{A,zenith} = T_{A,load} + G(V_{zenith} - V_{load}), \tag{3}$$

where V_{zenith} and V_{load} are the output voltages produced when the radiometer views the zenith and reference load respectively, and G is the gain calibration of the radiometer. We use a liquid-helium-cooled reference load because the nearly equal antenna temperatures of the reference load and zenith minimize the effect of gain-calibration errors on the measured zenith temperature.

Radiation reaching a radiometer pointed at the zenith comes from a number of sources; we can approximate $T_{A,zenith}$ as the sum:

$$T_{A,zenith} = T_{A,CBR} + T_{galaxy} + T_{A,atm} + T_{ground} \tag{4}$$

or combining equations (3) and (4)

$$T_{A,CBR} = T_{A,load} + G(V_{zenith} - V_{load}) - T_{galaxy} - T_{A,atm} - T_{ground} \tag{5}$$

where $T_{A,CBR}$ is the antenna temperature of the cosmic background radiation, T_{galaxy} is the antenna temperature of radiation from the galaxy (due to synchrotron emission and thermal emission from HII regions and interstellar dust), T_{ground} is the terrestrial thermal radiation intercepted by the antenna sidelobes, and $T_{A,atm}$ is the vertical antenna temperature of the atmosphere, less a small term (< 40 mK) resulting from the attenuation of the incoming CBR. (This is the quantity physically measured in zenith scans.) Subtraction of these sources from $T_{A,zenith}$ leaves the antenna temperature of the cosmic background radiation as the residual.

We have designed the experiment to minimize the extraneous sources of radiation entering the receivers. Some sources, such as the atmosphere and the galaxy, could not be reduced to negligible levels by equipment design. Instead, we have measured them with the same radiometers used to measure $T_{A,zenith}$ in order to minimize the effects of gain-calibration errors. Atmospheric emission is determined by making observations at a number of zenith angles and correlating the radiometer output with the atmospheric column density observed at different angles. Galactic emission is measured from drift scans we have made at the longer wavelengths.

The wavelengths (frequencies) of the radiometers were chosen to cover the region where the CBR is expected to have distortions and where the CBR could be measured accurately. The 0.91-cm and 0.33-cm wavelengths are in atmospheric windows and span the range between the long-wavelength measurements in the Rayleigh-Jeans region and the high-frequency measurements at the peak and beyond. In addition to tying the measurements together they provide a baseline to compare with the long-wavelength measurements.

3. – DESCRIPTION OF EXPERIMENT AND APPARATUS

(a) Radiometers, mirrors, and ground screens

In the first phase of the experiment, five radiometers, operating at wavelengths of 12.0, 6.3, 3.0, 0.91, and 0.33 cm, were used to measure $T_{A,CBR}$. A sixth radiometer monitored atmospheric emission at 3.2 cm. All were fixed-frequency superheterodyne receivers operated with Dicke switching, and all had low-sidelobe, corrugated-horn antennas as inputs. Each radiometer, as configured in 1982, is described in previous papers (Sironi *et al.* 1984; Mandolesi *et al.* 1984, Partridge *et al.* 1984; Friedman *et al.* 1984; and De Amici *et al.* 1984).

After the July 1982 measurements, each of the radiometers was modified to improve the quality of the CBR measurement and the ease of operation. The ground shields on all the radiometers were improved to reduce the extraneous thermal radiation and RF interference entering the sidelobes of the antennas. In addition each radiometer had alterations specific to its operation. For example, the reference mirror on the 3.0-cm radiometer was moved lower and extended to ensure that more of the reference antenna beam was directed toward the zenith. The 0.91-cm radiometer was improved with stiffer and flatter mirrors and more accurate pointing capability for zenith-angle scans. The configuration of the 0.33-cm radiometer was changed to provide a 60-degree opening angle between the two antennas, so that atmospheric zenith-angle scans could be made without mirrors. After the September 1983 measurements additional alterations were made to the radiometers. Most of the alterations were minor, except for changes in the 3.0-cm radiometer so that its reference reflector could be removed to expose the rotating mirror previously used by the 3.2-cm atmospheric monitor.

The 10, 33 and 90 GHz radiometers include thermal control systems, mirrors, side screens and carts which rolled into place over the cold load for data-taking. All three radiometers share the same batteries as power supplies, digital data recording system and reference cold load. Each radiometer had an ambient-temperature blackbody load for gain calibration. Each ambient-temperature calibrator was kept outside with the radiometer before and during data taking and the individual load temperatures were automatically recorded every 16 seconds.

(1) 10-GHz Radiometer

Figure 1 shows the 10-GHz (3.0-cm wavelength) radiometer configuration. The 10-GHz radiometer uses a Dicke-switched superheterodyne receiver. The receiver has a system noise temperature of 490 K and a RF bandwidth of about 1 GHz. The rms noise fluctuations are about 50 mK for a one-second integration time. A detailed description of the 10-GHz receiver is provided by Friedman (1984). The radiometer has two low-sidelobe corrugated-horn antennas with 12.5° beamwidths. The two antennas are mounted at right (90°) angles to each other. The secondary reference antenna is horizontal pointing northward. It views the zenith through a reflector set at 45° to vertical. It can also view the elliptical, motorized mirror used previously by the 3.2-cm atmospheric monitor (Partridge *et al.* 1983). The elliptical aluminum reflector is mounted at 45° to a horizontal shaft coincident with the secondary antenna beam axis. The shaft is motor-driven with an automatic controller so that the radiometer could make unattended atmospheric zenith angle scans when the primary antenna is pointed upwards.

The radiometer is mounted on bearings so that it can rotate about the axis of the antenna pointing north. The primary antenna can then swing through 360° to view any zenith angle from the zenith to the cold load. A system of aluminum sheets and screens surrounded both antennas and reflectors to shield against thermal emission from the ground. These shields were increased beyond those of the previous year, in order to improve the measurement and to include the elliptical reflector.

Measurements were made by pointing the primary antenna at the cold load and then at the zenith. The difference between the output voltages was proportional to the antenna temperature difference between the targets. Atmospheric scans pointed the primary antenna through the sequence 40° west, 30° west, vertical, 30° east, and 40° east. The atmospheric scans ended with observation of the ambient temperature load, then the primary returned to the cold load to begin the sequence again. Each position was maintained for 32 seconds.

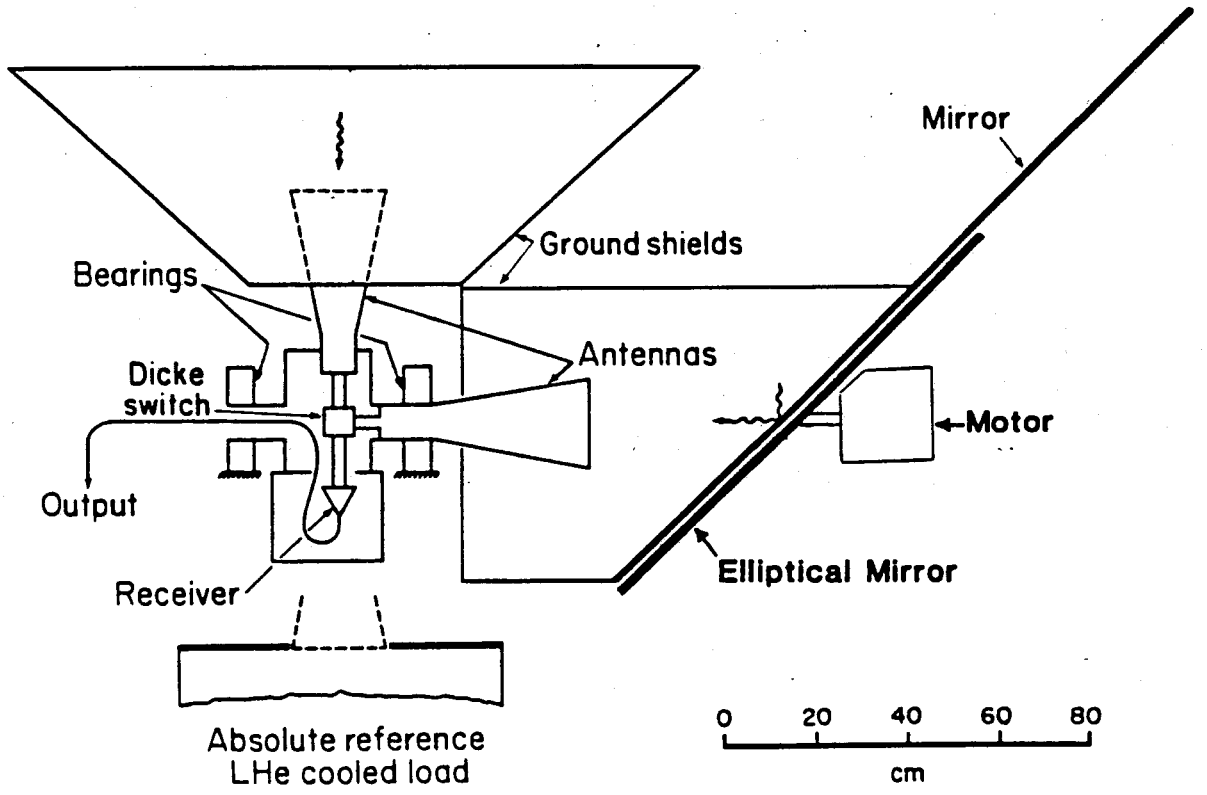

Figure 1. 10-GHz radiometer geometric configuration in 1984. The large fixed mirror was usually removed, exposing the rotating elliptical reflector and larger ground shields.

(2) 33-GHz Radiometer

Figure 2 shows the 33-GHz (0.91-cm wavelength) radiometer configuration. The basic design has changed very little since 1982. Two oppositely directed antennas provide inputs to the Dicke switch. The antennas are conical corrugated horns with a 7.5° beamwidth and low sidelobes. The Dicke switch operates at 100 Hz. The local-oscillator frequency is 32.91 GHz. The intermediate-frequency amplifiers have a bandwidth of 500 MHz. The antennas and receiver are mounted in an aluminum pipe, which is RF tight. The synchronous (lock-in) amplifier is located in the support electronics box attached to the cart. The lock-in demodulates, amplifies and integrates the signal for an interval of two seconds. Every two seconds the data-recording system digitizes and records the output. Thermal control systems, also located in the support electronics box, monitor and control the temperatures of the receiver and support electronics to prevent large changes in system gain. The radiometer and support electronics box are insulated with a styrofoam layer surrounding the RF enclosures.

The receiver is mounted on bearings to allow rotations in the North-South vertical plane. The receiver is pointed either vertically to measure the sky-cold load difference or horizontally to measure atmospheric emission by means of the mirrors, their pointing system and the ground screens. Each mirror consists of an aluminum honeycombed core sandwiched by two flat aluminum sheets and reinforced by channels along the edges. This design has proven to be very flat. The pointing system allows the orientation of the mirrors to be set at pre-selected angles to an accuracy of 2 arcminutes. Although the mirrors intercept nearly 100 percent of the beam pattern, the small spillover necessitates the use of ground screens to minimize the terrestrial thermal emissions intercepted by the antenna sidelobes. With the ground screens in place, the contribution T_{ground} is reduced to less than 30 mK even at the largest tilt angle.

The ambient-temperature calibration load is made of ferrite-loaded epoxy cast into an array of cones and embedded in foam insulation. Its reflection coefficient is less than $2\ 10^{-3}$. Its temperature typically changed less than 1° C per hour.

The data-taking cycle starts with the radiometer vertical so that one antenna points at the zenith and the other into the reference cold load. Then the radiometer is rotated 180° to interchange the antennas. The difference between these two observations is twice the difference in the power received from the sky and the cold load. The sum is twice the imbalance or offset of the radiometer. It is clearly important to construct the radiometer so that it has the same offset pointing upwards or downwards. For atmospheric scans the receiver is oriented horizontally and the mirror angles changed sequentially so that the antennas receive radiation from varying amounts of atmosphere. The observed zenith angles are 0°, 40°, and 50°. Gain calibrations are made by measuring the difference in output from the ambient temperature load and the cold load.

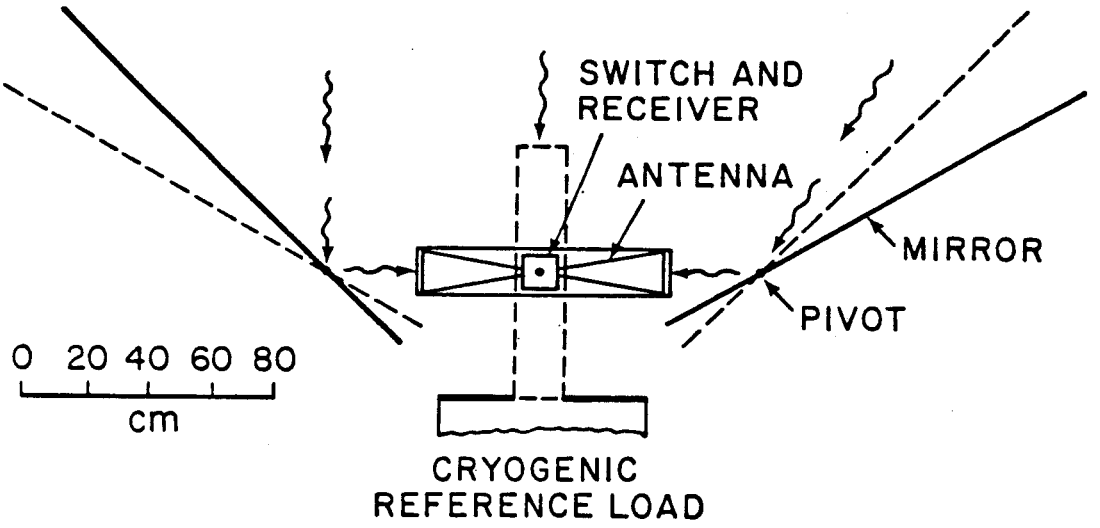

Figure 2. 33-GHz radiometer geometric configuration. The radiometer, shown oriented horizontally, makes zenith scans when the mirrors are tilted about pivot points aligned with the antenna beam axes. The radiometer rotates to point vertically for zenith-versus-cold-load measurements, as shown in the dashed outline.

(3) 90-GHz Radiometer

Figure 3 shows the 90-GHz (0.33-cm wavelength) radiometer configuration. In 1982 the 90-GHz radiometer topology was similar to that of the 33-GHz radiometer with the two antennas pointed in opposite directions; they now point 60° apart. This change improves the measurements of the atmospheric antenna temperature, $T_{A,atm}$, which places by far the most serious limitation on the CBR measurement at this frequency. Because the radiometer can be moved quickly from one position to another, little time is lost while the position is reset, so rapid measurements of the atmosphere can be made at several zenith angles. The radiometer configuration has the additional advantage that the zenith angles observed by the antennas during atmospheric measurements are determined only by the orientations of the antennas themselves and do not depend on the flatness and orientation of a reflector. Since an accurate measurement of $T_{A,atm}$ at 90 GHz requires with which the zenith angles be known to a few arcminutes, the ease and accuracy that the zenith angles can be measured in this configuration leads to more precise measurements of $T_{A,atm}$ and T_{CBR} (Witebsky, 1985).

During measurements of the zenith temperature both antennas point down, one antenna looks into the cold load while the other views the zenith by means of a reflector. The radiometer, which is mounted on bearings, is then rotated by 60° to reverse the roles of the two antennas and thereby remove the effects of radiometer offset. The atmospheric antenna temperature, $T_{A,atm}$, is obtained from observations at multiple zenith angles. The radiometer is rotated to point the antennas upward and stepped through a series of angles which cause the north antenna to view the sky at zenith angles of 50°, 40°, 20°, and 10° to the north of the zenith while its southern partner observes the complementary zenith angles 10°, 20°, 40°, and 50° south. Observations to the north and south are combined to remove radiometer offset and to reduce the effect of large-scale gradients in atmospheric humidity. Gain-calibration and data-recording techniques are much the same as those used with the 33-GHz radiometer. The lock-in amplifier has a two-second integration period, each pair of targets is observed for either 16 or 32 seconds, and a measurement cycle, consisting of observations of the zenith and cold load, a gain calibration, and a set of atmospheric measurements, takes 192 seconds.

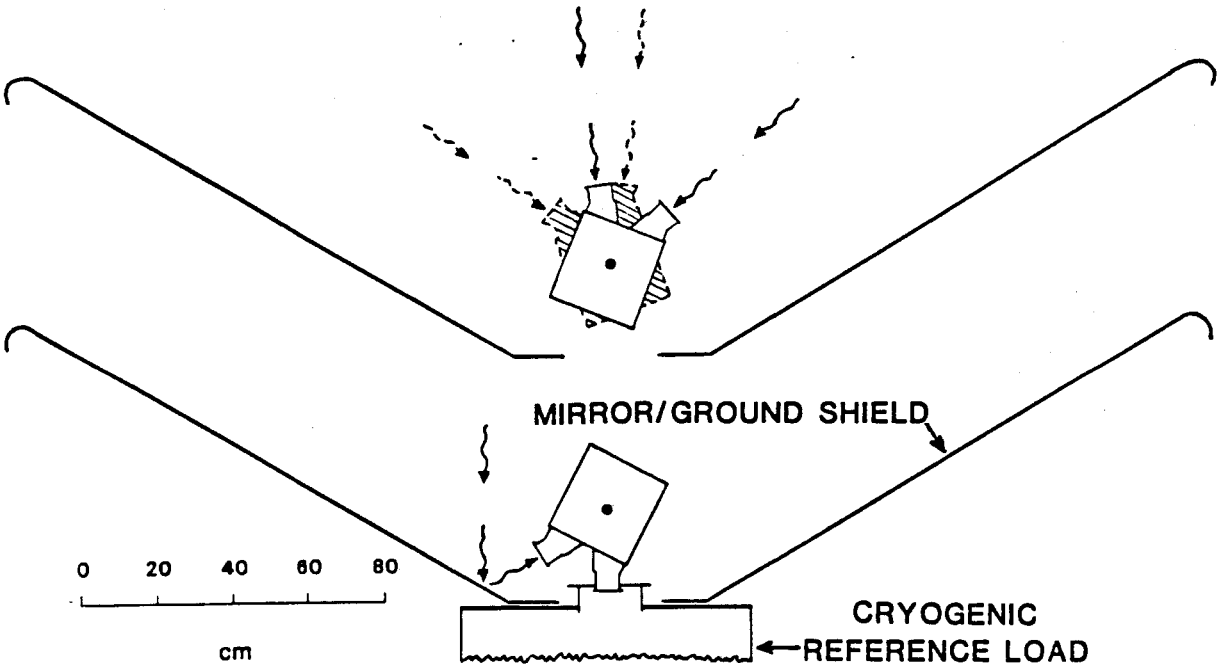

Figure 3. 90-GHz radiometer geometric configuration. (Top) To measure atmospheric emission one antenna points near the zenith (10° here) while the other antenna points to a larger zenith angle (50°) . The radiometer rotates to the symmetric position (shaded).
(Bottom) In sky-versus-cold-load measurements, one antenna views the cold load directly while the other observes the zenith in reflection. The radiometer rotates 60° counter-clockwise to reverse the roles of the two antennas.

(4) The Tunable 2-18 GHz Radiometer

Figure 4 illustrates the geometry of the tunable radiometer. The radiometer is enclosed in a metal housing insulated by a styrofoam lined cover which helps maintain thermal control. The metal housing helps to protect against RF interference and provides rigidity to the radiometer. The central part of the housing is a thick aluminum pipe in which two very broadband antennas are mounted pointing in opposite directions. Attached to this pipe on either end are two aluminum cones. These cones act as extensions of the antennas and help to define the beams. The radiometer assembly is mounted on a cart through two bearings that allow the radiometer to rotate in a vertical plane aligned north-south. When the radiometer is horizontal, each antenna faces a tiltable reflector. Each reflector has additional ground shields and a shield which fits between the lower part of the reflector and the bottom of the radiometer. When the radiometer is vertical, a nested pair of large aluminum cones can be lowered into position above the upper antenna to further define the beam and act as a ground shield. The lower antenna points downward and observes whatever target is placed there - e.g. the liquid-helium cold load, an ambient temperature load, a liquid-nitrogen-cooled load.

The tunable radiometer consists of two separate Dicke-switched radiometers contained within the single housing, and sharing the opposing antennas. The two radiometers receive orthogonal polarizations and are alternately connected to each antenna. In this way each radiometer is always receiving radiation from the antenna not connected to the other radiometer.

The radiometers operate over the frequency ranges 2-8 GHz (15 to 4 cm wavelength) and 7.5-18 GHz (4 to 1.7 cm). Each radiometer has an electronically controlled bandpass filter. A computer controls the filter frequency and records the radiometer output and various housekeeping information.

Figure 5 is a block diagram of the tunable receivers. Microwave radiation entering the antennas goes to the PIN-diode Dicke switch. The switch alternately connects the input of the first GaAs FET amplifier to the output port of each antenna. The signal, amplified by about 40 dB, passes through the YIG (Ytterium Iron Garnet) bandpass filter. The filtered signal is then amplified by another GaAs FET amplifier. The detector diode produces an output voltage proportional to the input power. A lock-in amplifier detects and amplifies the signal synchronous with the switching from one antenna to the other. The lock-in output is a noisy DC signal proportional to the difference in power received by the two antennas. After integration for 0.1 second, the signal is digitized and sent to the computer. The computer averages ten 0.1-second signals and records the average and rms.

The bandpass of the YIG filter is determined by the magnetic field in which the YIG spheres are suspended. This field is produced by a fixed coil and is thus proportional to the drive current. An analog driver circuit converts voltage to drive current. It corrects for the slight non-linearity of frequency versus drive current so that the frequency selected is very nearly proportional to the input voltage. The computer sets the frequency determining voltages by using two 8-bit digital-to-analog converters (DAC). There are thus 256 separate frequency settings in each of the two frequency ranges - 2-8 and 7.5-18 GHz. This represents an over sampling of about a factor of two in the 2-8 GHz range and five in the 8-18 GHz range.

In normal operation, a computer program sweeps each of the two filters through its tuning range, recording the radiometer output. It then informs the operator to rotate the radiometer so that the antennas are interchanged. Once the interchange is completed the computer sweeps through the frequency range again recording the data. This process is repeated until there are four runs with antenna A looking at the liquid-helium-cooled target interleaved with four runs with antenna A looking at the zenith. Since antenna B opposes antenna A it observes the same targets but out of phase. Atmospheric scans are accomplished in the same manner and with the same program except that the radiometer is fixed horizontally and the north and south reflectors are alternately raised and lowered. Gain calibrations are accomplished with an ambient temperature load in a similar manner but with fewer runs.

The 2-8 GHz radiometer has a representative system temperature of 1000 K and a bandwidth of 70 MHz for an rms sensitivity of 0.2 K for one second of integration. The 7.5-18 GHz radiometer has a representative system temperature of 1500 K and a bandwidth of 150 MHz for a one second integration time rms sensitivity of 0.2 K.

In order to check the performance of each radiometer several tests were made,some of which were periodically repeated. These tests include magnetic sensitivity tests, flip-offset tests, integration

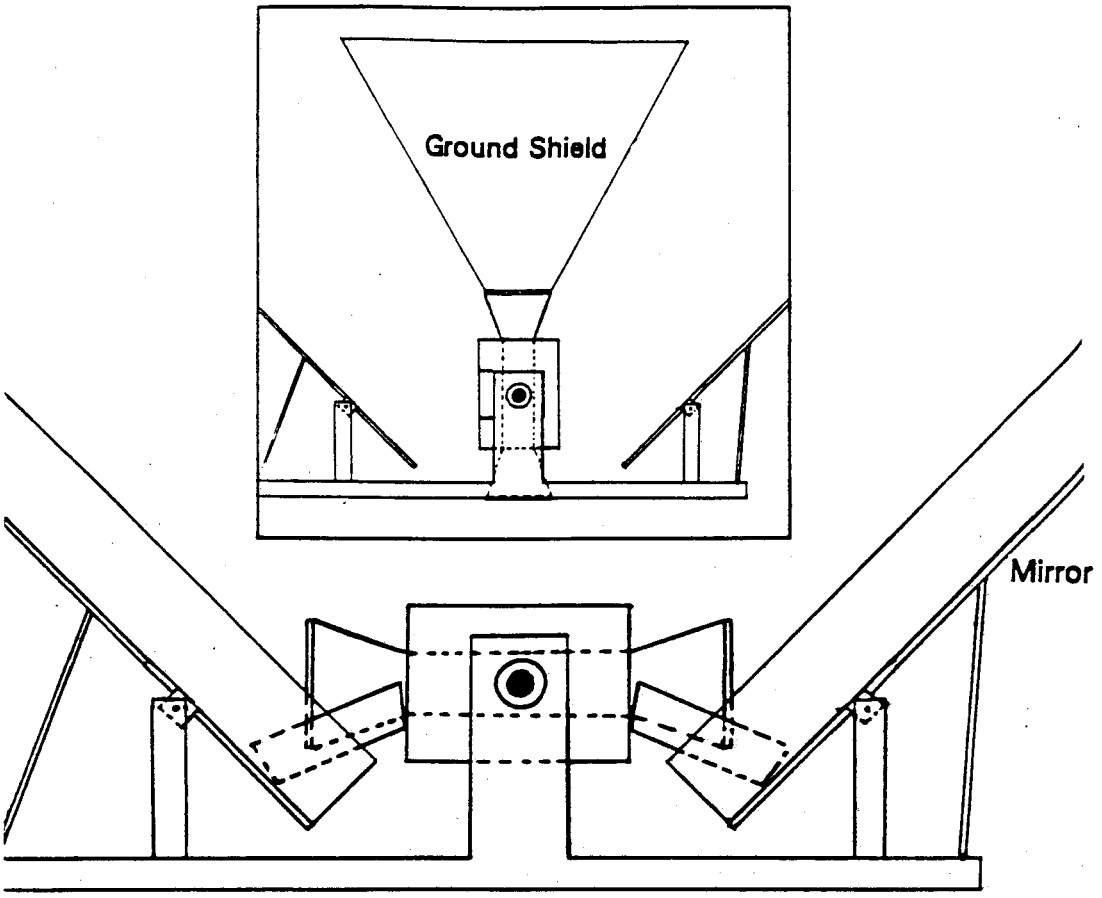

Figure 4. Tunable radiometer geometric configuration. (Top) In sky versus cold load measurements one antenna points into the cold load while the other views the zenith through the large conical ground shield. Then the radiometer is rotated 180° so that the antennas exchange places. (Bottom) For atmospheric scans the antennas point horizontally and the reflectors and side shields are tilted in turn: Large end screens (not shown) are fixed to the ground and do not move.

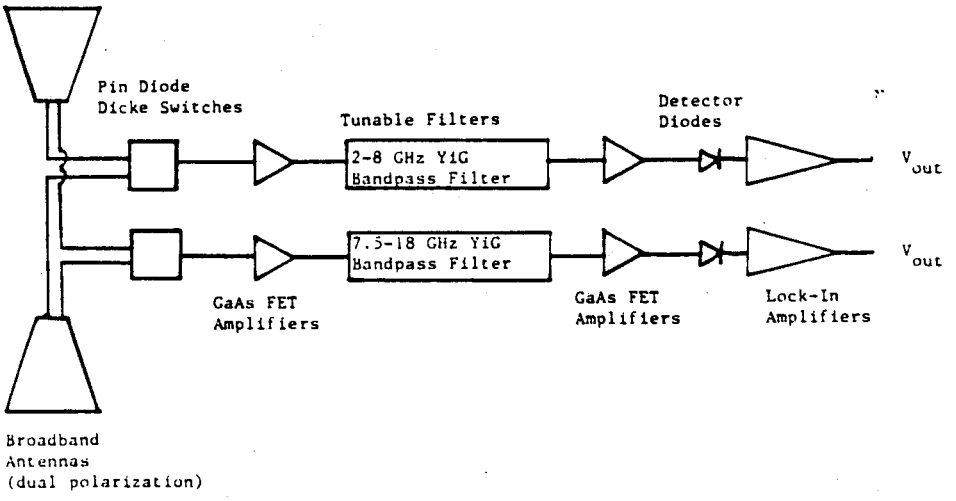

Figure 5. Tunable Radiometer Receivers Circuit Schematic. The 2-8 GHz and 7.5-18 GHz receivers share a common housing and the two antennas. The Dicke switches are synchronous with opposite phase, so that the receivers are always connected to separate antennas.

tests, gain stability tests, sidelobe tests and radio frequency interference tests. The magnetic sensitivity test, which tested the sensitivity of the radiometer to its orientation in the earth's magnetic field, yielded an effect well within the noise of the radiometers. Similarly, the flip-offset test, designed to test the receiver's sensitivity to the manual rotations, periodically performed during our measurements, also yielded results well within the noise level. The results of the gain stability tests indicate that the gain of the radiometers does not drift by more than 0.1 percent during a 17 minute period. The point-to-point fluctuations of the output of the radiometer can easily be accounted for by fluctuations in the sources pointed at, indicating that the gain is sufficiently stable. Although small, the signal intercepted by the antenna sidelobes, measured by the side lobe tests, is accounted for during the analysis of the data. Finally, the radio frequency interference tests indicated that the amplifiers were sufficiently well shielded from external man made radio sources.

(b) Absolute Reference Cold Load

The absolute reference cold load is an ambient-pressure liquid-helium-cooled target viewed through a large (0.7-m) open-mouth dewar covered by two windows of 23-micron-thick polyethylene film. The cold load has been described previously (Smoot *et al.* 1983) and has not been significantly modified. The pressure in the cold load was 488.5 ± 2.5 mm Hg, corresponding to a liquid helium boiling temperature of 3.778 ± 0.005 K. This is about 1 mm Hg higher and thus 0.002 K warmer than in 1982 and 1983. We calculate the emission from the absolute reference cold load for each frequency by converting this target temperature to antenna temperature and adding the emission from the windows and walls and the emission from the radiometer as reflected by the cold load. The reflection coefficient of the load is small, typically 10^{-3} or less.

4. – OBSERVATIONS

We made observations from the University of California White Mountain Research Station, a high (3800 m), dry (≤ 3 mm H_2O) site where atmospheric emission is reduced by approximately a factor of three compared to sea level. Its remote location reduced man-made RF interference in our measurement bands to acceptably low levels. The cart-mounted radiometers were positioned along a 20-m length of rails which are aligned east-west. Each cart in turn was rolled into position above the reference cold load and each radiometer then made a rapid series of measurements viewing the cold load and the sky both toward the zenith and at various angles from the zenith. The other radiometers made simultaneous atmospheric scans so we could compare measurements of atmospheric emissions at the various frequencies.

Observations were made with liquid helium in the cold load on the nights of 5 and 6 July 1982, 4, 5, and 6 September 1983 and 24 and 25 August 1984 UT. Observations with liquid nitrogen in the cold load were made on 4 and 7 July 1982, on 30 August, on 1,2, and 7 September 1983 and 17, 18, 23 August 1984 for practice and to crosscheck radiometer performance. August 1984 did not have an extended period of good dry weather as had previously occurred. This reduced our opportunity to obtain statistics on atmospheric stability.

5. – DATA REDUCTION

The data from the radiometers, the cold load, and housekeeping monitors were recorded on magnetic tape and disks in computer-compatible form. The major portion of data reduction was selecting the data from the tests, atmospheric scans, CBR measurements, etc. and averaging the data for each observation. Typically this meant excluding the first one or two data points (few seconds) for each observation to ensure that the radiometer or target was in place. After inspection, computer programs edited and averaged the data for each observation. The tunable radiometer's data did not need this editing procedure, since the computer did not record data during movement of the radiometer or changing of targets. The averaged data were reviewed, compared to other and previous measurements and saved for data analysis.

6. – DATA ANALYSIS

Each radiometer used a separate but basically similar algorithm for converting the zenith versus cold-load measurements, zenith scans, and gain-calibration measurements into a single measurement of $T_{A,atm}$ and $T_{A,CBR}$. For the tunable radiometer the data at each frequency were averaged for each of the two sets of four runs. The two averages were differenced and corrected for gain as a function

of frequency to provide the temperature difference between the zenith and the cold load. The zenith scan data were fitted to $T_{A,atm}$ taking into account the measured zenith angles, self-absorption by the atmosphere, the curvature of the atmosphere, the antenna's beam pattern, the value of T_{galaxy} at each zenith angle at the time of observation, and diffracted ground emission. Corrections are made for the polarization effects (angle dependent emissions) of the reflectors. Reflectors were involved in many of the atmospheric scans either because the secondary viewed the zenith through a mirror or because the mirrors directed the antenna beams through different amounts of atmosphere. The mirrors were made of clean aluminum and had very low emissivity ($< 10^{-3}$), as measured by a variety of means. However, this emissivity has polarization and angular dependence:

$$\epsilon_{perpendicular} = 4\pi\frac{\delta}{\lambda}cos\theta \tag{6}$$

$$\epsilon_{parallel} = 4\pi\frac{\delta}{\lambda}sec\theta \tag{7}$$

where perpendicular and parallel refer to the polarization orientation relative to the plane of scattering, θ is the incidence angle, δ is the skin depth and λ is the wavelength. For the antennas that were rotated with respect to their mirrors we minimized these effects by using circular polarization. Adjusting the plane of linear polarization minimized the change in emissivity for mirrors that were tilted. We then corrected for the residual effects which were typically on the order of 30 mK.

7. – SOURCES OF RADIATION AND SYSTEMATIC ERRORS

The galactic background is minimized by observations at high galactic latitudes and is estimated by scans and modeling. Values of T_{galaxy} are based upon measurements from the 12-cm and 6.3-cm radiometers and published data (e.g. Haslam et al, 1982). The data from the 12-cm, 6.3-cm, and 3.2-cm radiometers are in good agreement with the published data and simple frequency-scaling relations. We scaled the 12-cm results and our model by frequency to the 2.8 power, $\nu^{-2.8}$, to calculate T_{galaxy} for the tunable radiometer observations. Although this procedure is approximately valid only for the galactic synchrotron emission and not the other components of galactic emission, the net error is negligible.

Limits on ground emission are estimated by numerical integration of the measured antenna beam patterns and verified by tests to determine the effect of additional shields. We looked for coherent RF interference using the radiometers and also using a spectrum analyzer. The only RF interference found was observed with the 3.2-cm radiometer two days before the liquid-helium runs in 1982.

Flip offsets, that is changes in radiometer output depending upon the direction of observation, are an important problem. They directly affect the measurement of the temperature difference between the zenith and the reference cold load because the radiometer must be moved during the measurement. The corrections and uncertainties due to flip offsets caused by rotation from observing the cold load to observing the zenith are small. Flip offsets can also cause errors in the measurement of atmospheric emission; these errors are included in the estimates of $T_{A,atm}$ and its error. The 12-cm, 6.3-cm, and 3-cm radiometers had to be rotated to measure the atmospheric emission, as did the 0.33-cm radiometer in 1983 and 1984. The 33-GHz and tunable radiometers accomplished their zenith-angle scans with moveable mirrors.

Atmospheric emission is the largest background source in the experiment. For that reason we have attempted to measure the atmospheric emission very accurately. The radiometers were modified to improve their pointing accuracy during zenith-angle scans and to permit them to scan more quickly. In addition, we have changed our procedures to permit scans at multiple angles. In 1983 special efforts were made to obtain a large number of atmospheric measurements and to make some of them simultaneously at all six wavelengths. These improvements gave us more accurate atmospheric data with more cross-checks than in 1982. We were also fortunate that less water vapor was present during the September 1983 measurements than during those of July 1982, so the total atmospheric emission and variability were reduced. In 1984 we made simultaneous measurements of the atmosphere with the fixed-frequency radiometers during each run of a radiometer on the cold load and on several other occasions. The change in atmospheric temperature measured by one radiometer correlated well with the changes measured by the others (Costales 1984).

8. – RESULTS, COMPARISON TO PREVIOUS MEASUREMENTS AND INTERPRETATION

The measured atmospheric emission and our atmospheric emission model are shown in Figure 6 for the low frequency range. The measured antenna and thermodynamic CBR temperatures are listed in Table 1 along with the measured $T_{A,atm}$. Our fixed-frequency results are shown in Figure 7 along with other published measurements (see the review by Weiss, 1980; Meyer and Jura 1984). The results of this experiment agree well with previous measurements. The weighted average of our combined measurements is 2.73 ± 0.05 K, compared with 2.74 ± 0.09 K for the previous data. Our data and the data of Meyer and Jura (1984) are in conflict with those of Woody and Richards (1979, 1981). The preliminary new data of Peterson, Richards, and Timusk (1984) are compatible with all the results. With the exception of the Woody and Richards data all of the measurements fit a Planckian spectrum of temperature 2.73 ± 0.04 K with a Chi-squared of 9 for 22 degrees of freedom.

Our data alone, as well as with all the measurements in the Rayleigh-Jeans region, are consistent with a blackbody spectrum. A fit of the data to a blackbody spectrum plus a small Bose-Einstein distortion is inconsistent with any distortion characterized by a chemical potential larger than 10^{-2}. Such a distortion would deviate from blackbody spectrum by less than 6% in the most extreme model (Danese and De Zotti, 1982).

The tunable radiometer results are shown in Figure 8. These data are limited by systematic errors which we estimate to be about ± 0.5 K. We believe the primary cause of the systematic errors is reflection at the interface between the ends of the antenna and the cold load. Because the antennas are so broadband the impedance was not extremely well matched over the full frequency range. A small change in the impedance matching will partially reflect the approximately 250 K emitted by the receiver.

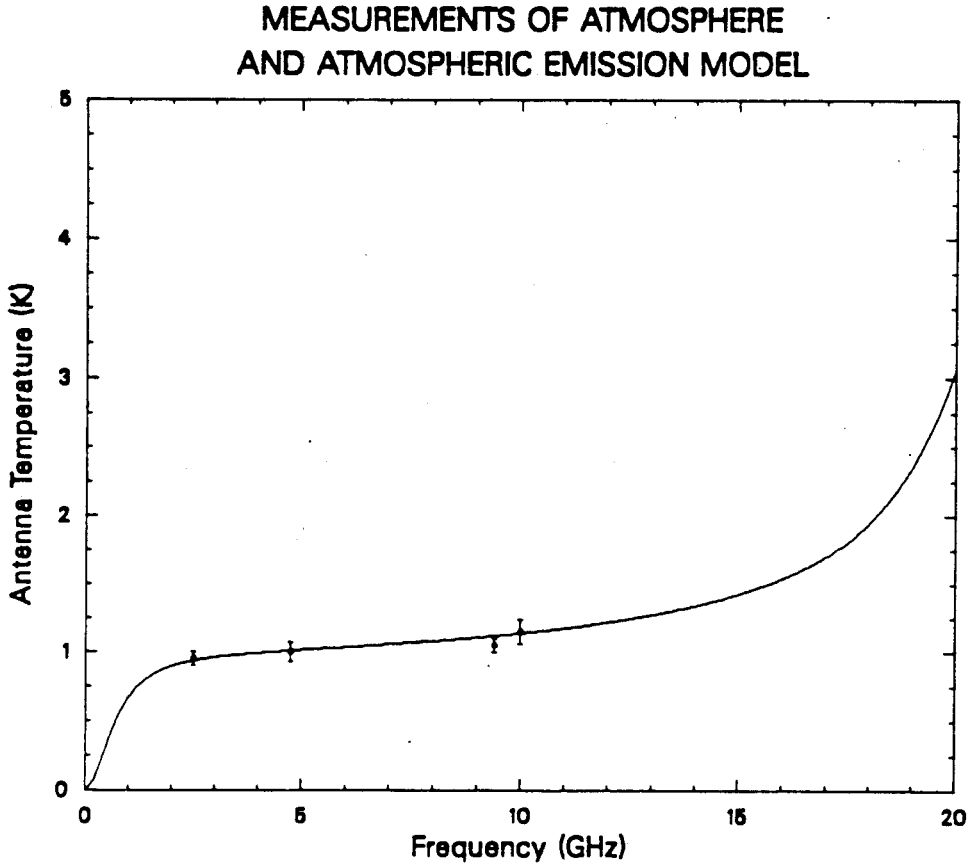

Figure 6. Atmospheric Emission Measurements and Model at White Mountain. The values measured at the four lowest fixed frequencies are in good agreement with the model, which assumes 3mm of precipitable H_2O.

Wavelength (cm)	Number of Observations	$T_{A,atm}$	$T_{A,CBR}$	T_{CBR} Thermodynamic	Combined Results
12.0	6	0.95 ± 0.05	2.49 ± 0.24	2.55 ± 0.24	
	18	0.95 ± 0.05	2.82 ± 0.15	2.88 ± 0.16	2.78 ± 0.13
6.3	5	1.0 ± 0.1	2.64 ± 0.21	2.74 ± 0.22	
	38	1.00 ± 0.07	2.60 ± 0.08	2.71 ± 0.08	2.71 ± 0.08
3.0	82	0.93 ± 0.16	2.68 ± 0.17	2.91 ± 0.17	
	59	1.20 ± 0.13	2.41 ± 0.14	2.64 ± 0.14	2.75 ± 0.08
	34	1.15 ± 0.09	2.46 ± 0.10	2.70 ± 0.13	
0.91	21	4.85 ± 0.14	2.10 ± 0.20	2.82 ± 0.21	
	32	4.53 ± 0.09	2.09 ± 0.13	2.81 ± 0.14	2.81 ± 0.12
	36	4.34 ± 0.09	2.09 ± 0.13	2.81 ± 0.14	
0.33	29	12.6 ± 0.59	0.86 ± 0.70	2.42 ± 1.00	
	49	9.87 ± 0.09	0.99 ± 0.11	2.57 ± 0.14	2.57 ± 0.14
	44	11.3 ± 0.13	1.00 ± 0.15	2.58 ± 0.19	

Table 1: Results of our fixed-frequency measurements of the CBR expressed in Kelvins. The first row at each wavelength is for the 1982 measurements; the second for 1983; the third for 1984.

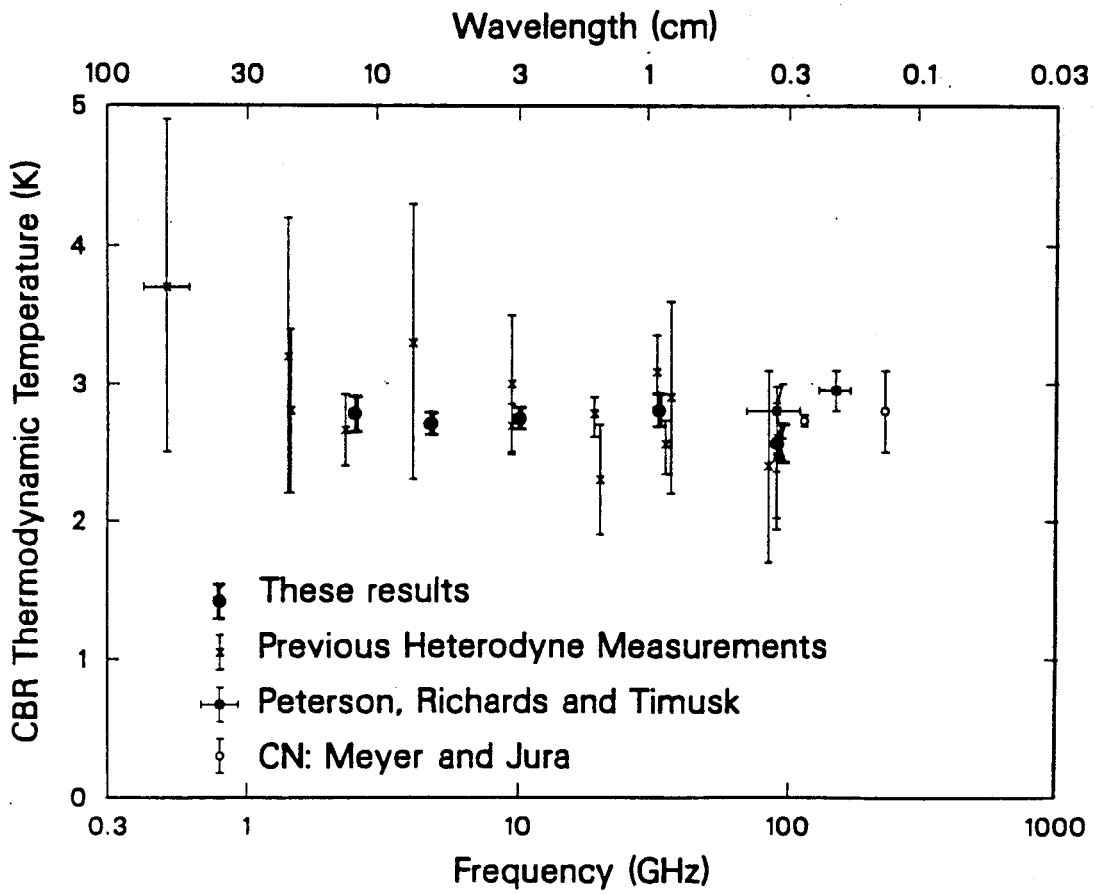

Figure 7. Plot of our fixed-frequency results together with previous measurements of the thermodynamic temperature of the cosmic background radiation.

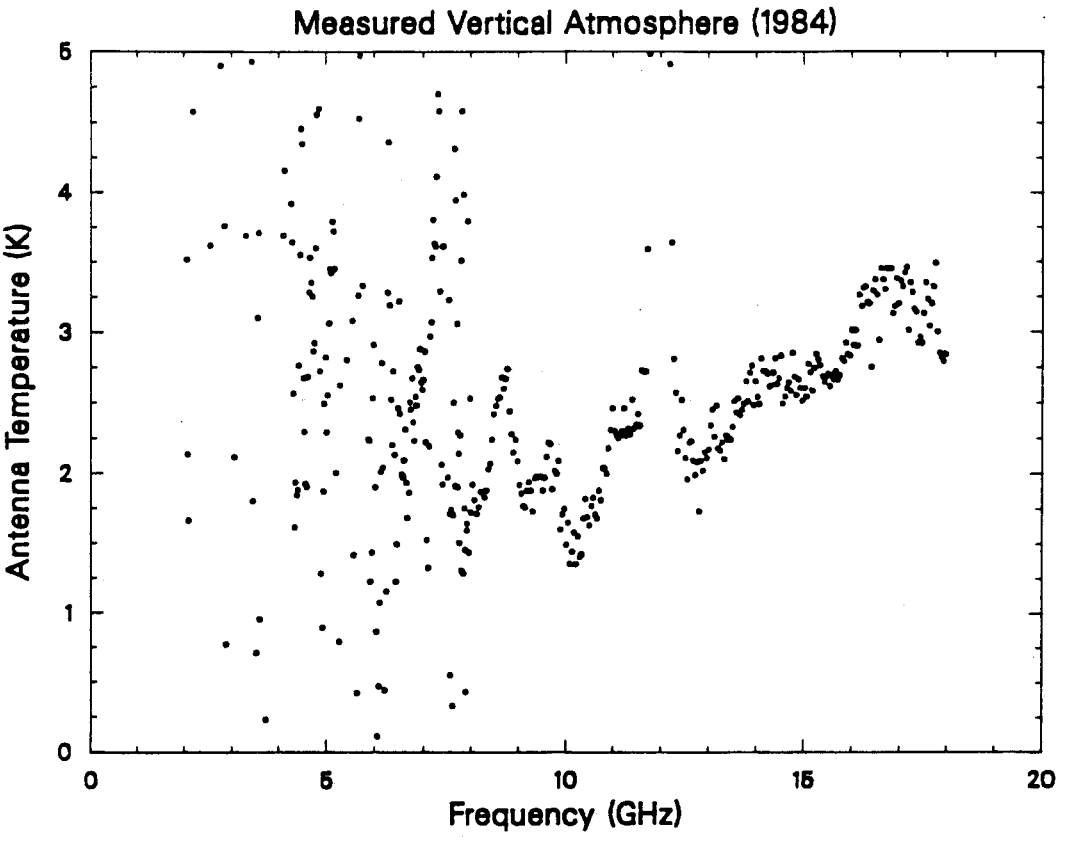

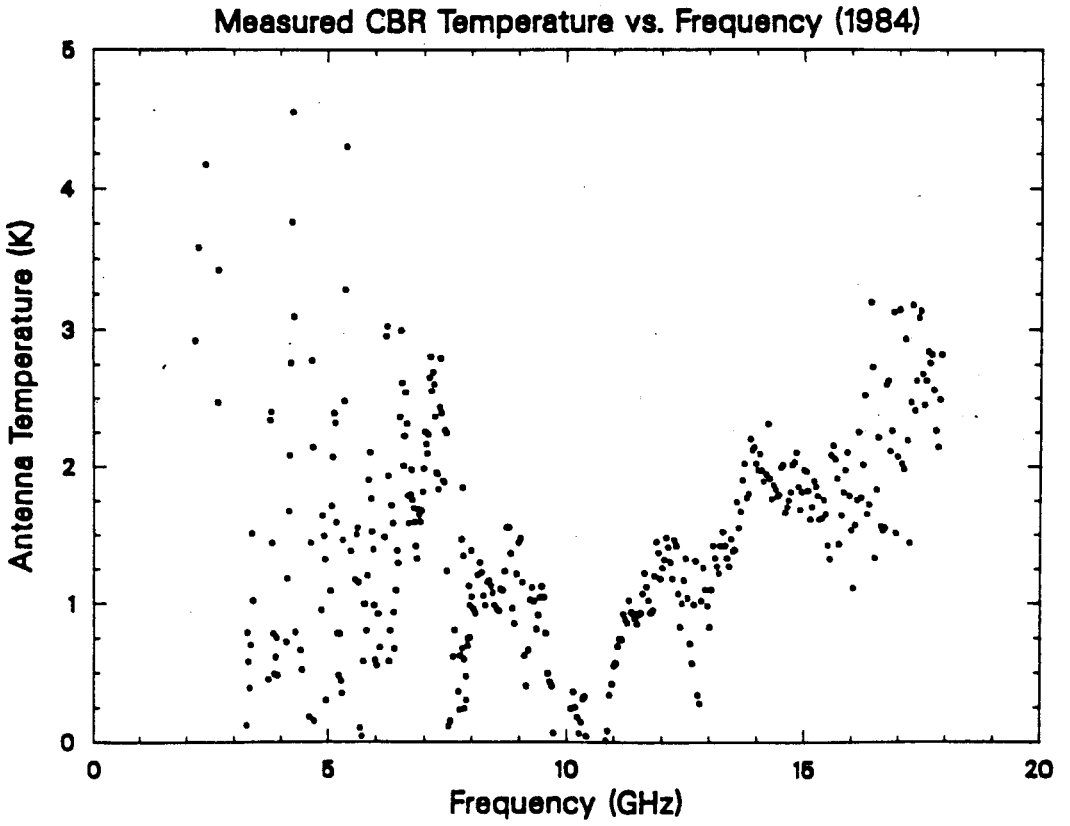

Figure 8. Plot of the tunable radiometer results.

9. – Future Work

We are improving our understanding of the radiometers and experiment. We are continuing the data analysis to refine the preliminary results presented here. We have determined that the quarter-wave plate, used to make the 10-GHz reference antenna circularly polarized, caused larger effects in the results of the atmospheric emission measurements than it should. We plan to make additional measurements of and with the 10-GHz radiometer in order to better understand and refine the atmospheric emission measurements. We are studying and rebuilding the tunable radiometer in an effort to improve its performance. If we improve these radiometers sufficiently, we will return to the White Mountain Research Station to make new measurements in the summer of 1985.

Other efforts are underway to measure the middle and high frequency portion of the CBR spectrum. In particular there is the far infrared spectrometer (FIRAS) which will be flown on the Cosmic Background Explorer (CoBE) satellite. John Mather (Goddard Space Flight Center) is the principal investigator and our group is involved as co-experimenters.

Acknowledgements: We thank the staff of the White Mountain Research Station and Hal Dougherty, John Gibson, Jim Costales, Mark Griffith, Bruce Grossan, Linda Kelley, and Faye Mitschang for their assistance.

This research was supported by National Science Foundation Grants No. PHY80-15694 and AST 800737, by the Department of Energy under Contract DE-AC03-76SF00098, and by Italian Consiglio Nazionale delle Ricerche Fellowships No. 203.2.13 and 203.2.15, and by Italian Ministero Della Pubblica Istruzione.

REFERENCES

Costales, J. 1984, Senior Thesis and Lawrence Berkeley Laboratory Report LBL-18744.
De Amici, G., Witebsky, C., Smoot, G., and Friedman, S. 1984, *Phys. Rev. D* **29**, 2673.
Danese, L. and De Zotti G. 1977, *Riv. Nuovo Cimento* **7**, 277.
Danese, L. and De Zotti G. 1978, *Astron. Astrophys.* **68**, 157.
Danese, L. and De Zotti G. 1982, *Astron. Astrophys.* **107**, 39.
Friedman, S. D., Smoot, G. F., De Amici, G., and Witebsky, C. 1984, *Phys. Rev. D* **29**, 2677.
Friedman, S. D. 1984, Ph. D. Thesis and Lawrence Berkeley Lab Report LBL-17279.
Haslam, C. G. T., *et al.* 1982, *Astron. Astrophys. Supp. Series* **47**, 1.
Illarionov, A. F. and Sunyaev, R. A. 1975, *Sov. Astron.* **18**, 691.
Mandolesi, N., *et al.* 1984, *Phys. Rev. D* **29**, 2680.
Meyer, D. M. and Jura, M. 1984, Ap. J. Lett. **276**, L1.
Partridge, R. B., *et al.* 1984, *Phys. Rev. D* **29**, 2683.
Sironi, G., *et al.* 1984, *Phys. Rev. D* **29**, 2686.
Smoot, G. F., *et al.* 1983, *Phys. Rev. Lett.* **51**, 1099.
Smoot, G. F., *et al.* submitted 1984, *Ap. J. Lett.* and LBL-18602.
Weiss R. 1980, *Annual Rev. Astron. Astrophys.* **18**, 489.
Witebsky, C. 1985, Ph. D. Thesis and Lawrence Berkeley Laboratory Report LBL-18746.
Woody, D. P., and Richards, P. L. 1979, *Phys. Rev. Lett.* **42**, 925.
Woody, D. P., and Richards, P. L. 1981, *Ap. J.* **248**, 18.